Polyoxometalates

DOI: 10.1002/anie.201008225

Molecular Growth of a Core–Shell Polyoxometalate**

Xikui Fang, Paul Kögerler,* Yuji Furukawa, Manfred Speldrich, and Marshall Luban*

The self-assembly of large metal oxide clusters usually proceeds via condensation steps thermodynamically driven by charge and nucleophilicity of the growing transient cluster fragments. Polyoxometalate (POM) chemistry[1] has accumulated many strategies to interfere with these basic formation principles, aiming at both directed molecular growth and targeted functionalization by selective introduction of metal centers or organic moieties. POM structures integrating 3d or 4d transition-metal ions in particular attest to this approach, and they have led to a rich class of molecular materials[2] ranging from molecular magnets[3] to oxidation catalysts.[4] In this context, polyoxotungstate clusters provide rigid and redox-stable scaffolds based on building-block-type fragments that are frequently derived from archetypal structures such as the Keggin, Dawson, or Lindqvist species.[5] Additional heterometal cations coordinating to or interconnecting these nucleophilic structures are key to the reactivity and the electronic and magnetic characteristics of the resulting adducts.[6] This situation is exemplified by the spherical $\{M_{72}L_{30}\}$ Keplerate clusters that have been realized both as polymolybdate (M = Mo) and polytungstate (M = W) structures containing a variety of heterometal linkers (L = V, Cr, Fe, etc.).[7] These clusters, comprising unique spin polytopes that represent molecular analogues of Kagomé lattices, constitute structural platforms for subsequent reactions, ranging from redox reactions[8] and partial heterometal exchange[9] to condensations to one- and two-dimensional coordination networks[10]—all of which alter the clusters' magnetic characteristics while retaining the basic cluster structure. Moreover, recent development of POM-based single-molecule magnets[3] raises the hope that magnetic POMs may find their way into areas such as molecular spintronics or quantum computing.[11]

However, the controlled growth of large metal oxide clusters remains elusive: precise prediction of the outcome is very difficult given the involvement of many, often labile, metal–oxygen bonds. The self-assembly mechanisms that underlie the formation of larger POMs in aqueous reaction solutions are barely established and are not compatible with the synthetic controls available in classical coordination chemistry, as exemplified by the use of molecular tectons, characterized by their specific connectivity constraints, in the rational production of supramolecular aggregates[12] or porous metal–organic frameworks.[13]

We postulate that this roadblock in controlling the molecular growth steps in polyoxotungstate chemistry can be partially circumvented by kinetic control of competing reactions, as illustrated by the template-induced formation of a 4.3 nm manganese(III) polyoxotungstate cluster anion $[Mn^{III}_{40}P_{32}W^{VI}_{224}O_{888}]^{144-}$ (**1**). The preparation of **1** starts from metastable $[\alpha\text{-}H_2P_2W_{12}O_{48}]^{12-}$ ($\{P_2W_{12}\}$), a hexavacant phosphotungstate derived from the plenary $[\alpha\text{-}P_2W_{18}O_{62}]^{6-}$ Dawson anion ($\{P_2W_{18}\}$) by base degradation.[14] Briefly, the synthesis of **1** is accomplished by dissolution of $\{P_2W_{12}\}$ in 1:1 HOAc/LiOAc, acidic conditions that are known to favor the $\{P_2W_{12}\}\rightarrow\{P_8W_{48}\}$ transformation.[15] Subsequent addition of $[Mn_{12}O_{12}(OAc)_{16}(H_2O)_4]\cdot 4H_2O\cdot 2HOAc$,[16] used widely as a source of Mn^{III} ions in the synthesis of various molecular magnets,[17] leads to slow formation of black crystals of $K_{56}Li_{74}H_{14}\mathbf{1}\cdot$ca.$680\,H_2O$ (**1a**) in an overall yield of 27%.

Compound **1a** crystallizes in the triclinic space group $P\bar{1}$ with two formula units per unit cell. The asymmetric unit contains the entire polyanion **1** and mostly disordered crystal water molecules and counterions, which account for nearly $^2/_3$ of the unit cell volume (ca. 67000 Å^3). The structural solution and refinement of **1a** approach dimensions common to protein crystallography. There are approximately 1500 unique atoms, and the final model uses more than 7500 parameters ($R_1 = 0.0953$, $wR_2 = 0.2228$).[18]

The crystal structure of **1a** (Figure 1) reveals a core–shell cluster aggregate formally constructed from a total of 16 corner-sharing Dawson-type units, formulated as $[(P_8W_{48}O_{184})\{(P_2W_{14}Mn_4O_{60})(P_2W_{15}Mn_3O_{58})_2\}_4]^{144-}$. With 224 tungsten centers, it is the largest known polyoxotungstate (diameter of the van der Waals surface: 43/43/34 Å). At the heart of **1** is a $\{P_8W_{48}\}$ core encapsulated by a shell of 12 Mn-substituted Dawson units. The entire 16-Dawson assembly has idealized S_4 symmetry, with the principal axis coinciding with the fourfold axis of the central $\{P_8W_{48}\}$ wheel. The outer shell is composed of four identical tri-Dawson subunits that are related by the non-crystallographic S_4/C_2 axis (Figure 1b), and each trimer is attached to a single $\{P_2W_{12}\}$ moiety of the $\{P_8W_{48}\}$ core. Two co-planar trimers (light blue in Figure 1)

[*] Dr. X. Fang, Prof. Dr. Y. Furukawa, Prof. Dr. M. Luban
US DOE Ames Laboratory
and
Department of Physics and Astronomy
Iowa State University
Ames, Iowa 50011 (USA)
Fax: (+1) 515-294-0689
E-mail: xfang@ameslab.gov
Prof. Dr. P. Kögerler, Dr. M. Speldrich
Institute of Inorganic Chemistry
RWTH Aachen University
52074 Aachen (Germany)
Fax: (+49) 241-80-92642
E-mail: paul.koegerler@ac.rwth-aachen.de

[**] We are grateful to Dr. Gordon Miller (Iowa State University) for granting access to X-ray facilities and Dr. Peter Müller (Massachusetts Institute of Technology) for helpful discussions on crystal structure refinement. Ames Laboratory is operated for the U.S. Department of Energy by Iowa State University under Contract No. DE-AC02-07CH11358.

Supporting information for this article is available on the WWW under http://dx.doi.org/10.1002/anie.201008225.

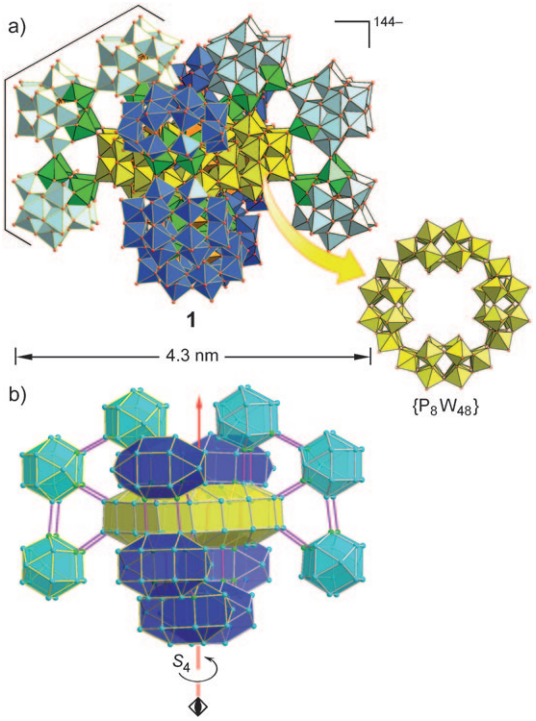

Figure 1. a) A polyhedral plot of **1** shows the central $\{P_8W_{48}\}$ template (yellow) and the four Dawson trimers, distinguished by edge colors and blue hues (one trimer emphasized by bordering lines), all of which are joined through Mn^{III} groups (green octahedra). b) The Mn/W metal skeleton from the same view direction highlighting Mn–O=W bonds (purple) and the orientation of the S_4 axis.

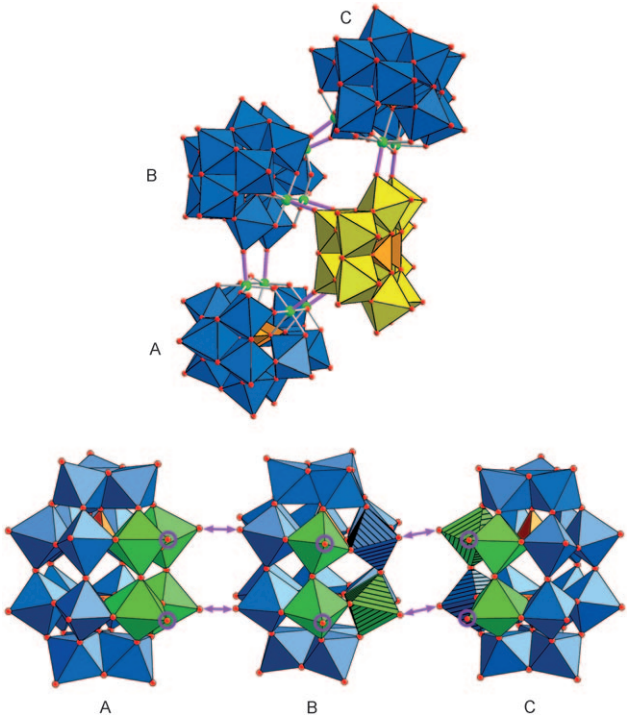

Figure 2. Top: Structure of a tri-Dawson subunit (blue) attached to a $\{P_2W_{12}\}$ fragment (yellow) of the central $\{P_8W_{48}\}$ ring. The bridging Mn–O(=W) bonds (purple) between the three Dawson constituents (A, B, and C) and $\{P_2W_{12}\}$ indicate the direction of JT axes of the Mn^{III} sites (green spheres). Bottom: Connectivity between the three Dawson units. Double arrows point to the oxygen positions involved in the (formal) condensation process that links neighboring Dawson units through dual Mn–O=W bridges. Hatched coordination octahedra: Mn/W sites affected by positional disorder. Encircled oxygen sites bridge the Dawson units and the central $\{P_8W_{48}\}$ ring (phosphate orange).

are appended to the $\{P_8W_{48}\}$ upper rim and are orthogonal to the remaining two trimers (dark blue) attached to the bottom rim, thus minimizing steric repulsion between the trimer units. The central hydrophilic $\{P_8W_{48}\}$ cavity is filled with solvent and counterions but no Mn ions.

Figure 2 illustrates the connectivity within one trimer subunit. Its three Dawson units (A, B, and C) are derived from the $\{P_2W_{12}\}$ anion by reconstituting either three (B, C) or four (A) of its vacant W sites with Mn ions; the remaining vacancies are filled with W atoms. Neighboring Dawson units share two corners through two parallel Mn–O=W bridges. The alternating dual bridging between units B and C shows crystallographic positional disorder with a Mn/W occupancy factor ratio of 50:50, a situation also observed in analogous di-[19] and tri-Dawson[20] systems. All of the Mn centers are in the valence state +III, as established by a combination of bond valence sum (BVS) calculations[21] and the presence of tetragonal Jahn–Teller (JT) elongations characteristic of high-spin d^4 ions in octahedral ligand environments. Note that all Mn–O=W bridges involve JT-elongated axial Mn–O bonds. Furthermore, data from X-ray photoelectron spectroscopy (XPS) suggests a uniform oxidation state for all Mn centers, with only two Mn 2p bands at 646.8 ($2p_{3/2}$) and 658.1 eV ($2p_{1/2}$).

A remarkable aspect in the molecular growth of **1** is the probable template effect of the central $\{P_8W_{48}\}$ wheel, whose surface serves as a likely starting point of cluster aggregation, although cluster growth rarely occurs on intact POM cluster surfaces. The d–p π-orbital overlap between early-transition-metal ions and the terminal oxo ligands produces strong M=O bonds that help retain structural integrity of POM clusters. On the other hand, it decreases the nucleophilicity of the M=O oxo ligands, and as a result, coordinative bonding to these sites is generally too labile to support robust growth of discrete clusters. In this context, the dual Mn–O=W bridging motif may emerge as an effective approach to compensate weak axial Mn–O bonds by introducing double or multiple bridges: The 40 Mn^{III} ions in **1** are involved in 20 dual Mn–O=W linkages through their JT-elongated axial bonds (ca. 2.2 Å), while the other four equatorial Mn–O bonds (ca. 1.9 Å) firmly anchor the Mn sites in their respective Dawson groups. Therefore, these dual bridges essentially serve as the backbone of the giant assembly.[22]

To rationalize the molecular growth of **1**, we postulate three concurrent reactions central to the formation of **1** that proceed with comparable rates under the selected reaction conditions (Figure 3):

1) The well-established formation of the D_{4h}-symmetric $[H_7P_8W_{48}O_{184}]^{33-}$ ($\{P_8W_{48}\}$) ring cluster structure from $\{P_2W_{12}\}$.[15]

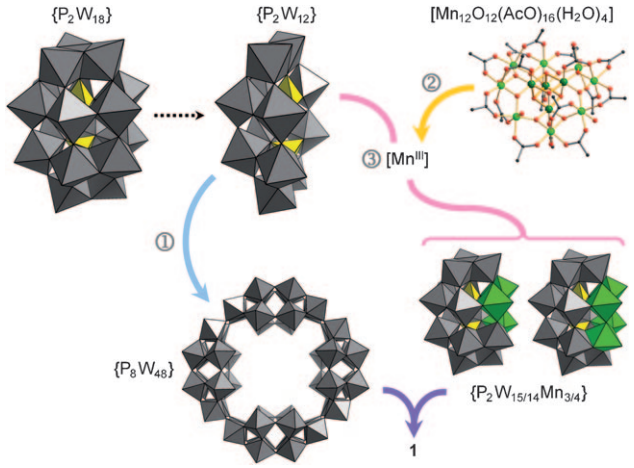

Figure 3. Postulated reaction steps in the formation of **1**.

2) The decomposition of $[Mn^{III/IV}{}_{12}O_{12}(OAc)_{16}(H_2O)_4]$ in aqueous solution, resulting in the release of intermediate Mn^{III} species.
3) The integration of Mn^{III} ions into $\{P_2W_{14}Mn^{III}{}_4\}$ and $\{P_2W_{15}Mn^{III}{}_3\}$ Dawson-type intermediates, which condense onto the outer surface of the $\{P_8W_{48}\}$ ring and one or two adjacent Dawson-type groups through Mn–O=W bridges.

Given the high reactivity of $\{P_2W_{12}\}$,[23] these groups are plausible targets for initial reaction with Mn^{III} (versus, for example, coordination of Mn^{III} to preformed $\{P_8W_{48}\}$ rings), and they also represent the most likely source for the additional one or two tungstate centers in $\{P_2W_{14}Mn_4\}$ and $\{P_2W_{15}Mn_3\}$.

On the basis of the experimental data, we cannot identify a precise sequence of steps that link these initial and secondary building blocks through Mn–O=W bridges to the final structure, in which four curved $\{P_2W_{14}Mn_4\}\{P_2W_{15}Mn_3\}_2$ Dawson trimers surround the central $\{P_8W_{48}\}$ ring to complete the $(\{P_2W_{14}Mn_4\}\{P_2W_{15}Mn_3\}_2)_4\{P_8W_{48}\}$ polyanion **1**. A templating function of $\{P_8W_{48}\}$, which potentially also accelerates the formation of the multiple Mn–O=W bridges, appears likely in this self-assembly of **1**. Note that this outward expansion of the $\{P_8W_{48}\}$ ring cluster represents a fundamental departure from all known discrete 3d-metal-ion-functionalized $\{P_8W_{48}\}$ species in which the heterometal ions are accumulated in the central cavity, thus resulting in magnetic aggregates such as $\{Cu^{II}{}_{20}\}$,[24] $\{V^{IV}{}_{12}\}$,[25] $\{Fe^{III}{}_{16}\}$,[26] $\{Co^{II}{}_{10}\}$,[27] or, in some rare cases, in infinite arrays.[28] Key to the outward growth appears to be the sufficiently slow production of low-nuclearity Mn^{III} intermediates. This situation prevents rapid reaction with all available $\{P_2W_{12}\}$ units and in turn allows for the competing formation of $\{P_8W_{48}\}$. It also avoids high Mn^{II} cation concentrations from subsequent disproportionation reactions ($2\,Mn^{III} \rightarrow Mn^{II} + Mn^{IV}$). No Mn^{II} cations are found as constituents in the cationic lattice of **1a**.

Magnetic susceptibility measurements indicate intramolecular antiferromagnetic coupling between the Mn^{III} spin centers. Owing to the high nuclearity and structural complexity of the Mn_{40} array, modeling the magnetism of **1** requires several simplifications in order to avoid overparametrization. The Mn_{40} spin polytope in **1** can be decomposed into four identical and independent Mn_{10} units present in each $\{(P_2W_{14}Mn_4O_{60})(P_2W_{15}Mn_3O_{58})_2\}$ trimer, and each of these Mn_{10} units consists of one Mn_4 rectangle and two Mn_3 triangles (Figure 4). In a Heisenberg model, three exchange coupling energies characterize the nearest-neighbor Mn···Mn contacts within these units: J_1 (exchange mediated by μ-O, O–P–O, and O–W–O bridges; Mn···Mn ca. 3.5 Å), J_2 (one μ-O bridge; ca. 3.7 Å), and J_3 (one O–W–O bridge; ca. 5.0 Å). Any coupling between the triangles and the rectangle (d(Mn···Mn) > 5.2 Å) is accounted for by a (purely empirical) molecular field parameter λ, defined as $\chi_{mol}{}^{-1} = \chi'_{mol}{}^{-1} - \lambda$ where χ'_{mol} represents the susceptibility as it results from the

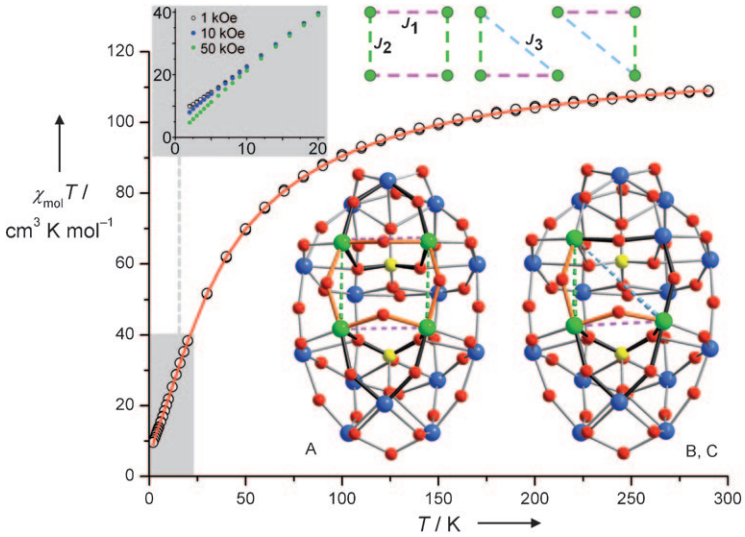

Figure 4. Temperature dependence of $\chi_{mol}T$ of **1a** at 0.1 T (circles: experimental data; red line: best fit to the Heisenberg Hamiltonian augmented by a molecular-field correction) and field-dependent low-temperature data showing the onset of magnetic saturation below ca. 15 K (gray background). One $\{P_2W_{14}Mn_4\}$ (left) and one $\{P_2W_{15}Mn_3\}$ unit (right) are shown highlighting the Mn–O–Mn bridges (orange bonds) and the Mn–O–P–O–Mn and Mn–O–W–O–Mn bridges (black bonds) that distinguish J_1 (purple), J_2 (green), and J_3 (blue dashed lines) contacts, as summarized in the coupling scheme for each Mn_{10} group (top). W blue, O red, Mn green, P yellow, terminal O omitted for clarity.

Heisenberg-type exchange model. Adopting an isotropic spin Hamiltonian for spin-only $S = 2$ centers (i.e., ignoring orbital contributions and approximating the Mn^{III} sites in their JT-distorted MnO_6 environments), the 0.1 Tesla susceptibility data is reproduced by the all-antiferromagnetic coupling scenario $J_1 = -2.20\ cm^{-1}$, $J_2 = -2.16\ cm^{-1}$, $J_3 = -1.30\ cm^{-1}$, and $\lambda = -0.066\ mol\,cm^{-3}$ ($g_{iso} = 1.995$).[29] Isospectrality issues (leading to identical fits for several sets of J_{1-3}) required us to employ fitting constraints for the ratios J_1/J_2 (1.0–0.9) and J_1/J_3 (1.0–0.5) that were based on plausible limits derived for the above-listed exchange pathways. The resulting exchange energies are well in line with other Mn^{III}-function-

alized POM structures. The value of $\chi_{mol}T$ does not drop to zero, as expected for a singlet ground state, when T is decreased down to 2 K. This behavior is due to the residual $S=1$ spin resulting for the discrete Mn_3 units that, in the lowest experimental temperature range, is not fully compensated by antiferromagnetic intertriangle coupling (λ). The residual spin also accounts for a decrease in the value of $\chi_{mol}T$ with increasing external field below 15 K owing to increasing magnetic saturation.

^{7}Li and ^{1}H solid-state NMR spectroscopy measurements elucidate the low-temperature magnetic properties of **1** from a complementary microscopic perspective. Signals in the ^{7}Li NMR spectra were detected at almost zero NMR shift ($K=(0.01\pm0.02)\,\%$) position and line widths (full width at half amplitude, FWHA) increase with decreasing temperature from $T=250$ K (FWHA $\approx$ 7.7 Oe) down to $T=1.6$ K (FWHA $\approx$ 117 Oe; see the Supporting Information). Similar broadening of the line width at low temperatures is also observed in ^{1}H NMR spectra. Since the ^{7}Li and ^{1}H NMR spectral line widths are mainly produced by dipolar field from Mn spins, the broadening at low temperatures provides direct evidence of non-vanishing Mn spin moments. Thus, these results from NMR spectroscopy are consistent with the uncompensated $S=1$ spins on the Mn_3 triangles at the experimental base temperature of 1.6 K.

In summary, the formation of the $\{Mn_{40}W_{224}\}$ polyanion **1** exemplifies the synthetic potential of combining supramolecular templating and kinetic competition approaches in the expansion of known POM base structures. The complex solid-state structure **1a** reflects how different archetypal building blocks can be anchored to each other through a network of dual Mn–O=W bridges, thus overcoming the lability otherwise inherent to coordination to W=O surface groups. We note that the template effect of the central $\{P_8W_{48}\}$ unit in **1** mirrors a more general characteristic of controlled molecular growth of giant POMs.[30] Importantly, the synthetic strategies derived from the formation of **1a** are in principle transferrable to a wide range of other POM architectures, and we expect further advances in molecular growth starting from known giant POM clusters.

Received: December 28, 2010
Published online: April 19, 2011

Keywords: cluster compounds · magnetic properties · polyoxometalates · template synthesis

[1] M. T. Pope, *Heteropoly and Isopoly Oxometalates*, Springer, Berlin, **1983**.

[2] a) D.-L. Long, R. Tsunashima, L. Cronin, *Angew. Chem.* **2010**, *122*, 1780–1803; *Angew. Chem. Int. Ed.* **2010**, *49*, 1736–1758; b) A. Proust, R. Thouvenot, P. Gouzerh, *Chem. Commun.* **2008**, 1837–1852.

[3] a) C. Ritchie, A. Ferguson, H. Nojiri, H. Miras, Y.-F. Song, D.-L. Long, E. Burkholder, M. Murrie, P. Kögerler, E. Brechin, L. Cronin, *Angew. Chem.* **2008**, *120*, 5691–5694; *Angew. Chem. Int. Ed.* **2008**, *47*, 5609–5612; b) M. A. AlDamen, J. M. Clemente-Juan, E. Coronado, C. Mart-Gastaldo, A. Gaita-Ario, *J. Am. Chem. Soc.* **2008**, *130*, 8874–8875.

[4] a) N. Mizuno, K. Kamata, K. Yamaguchi, *Top. Catal.* **2010**, *53*, 876–893; b) Q. Yin, J. M. Tan, C. Besson, Y. V. Geletii, D. G. Musaev, A. E. Kuznetsov, Z. Luo, K. I. Hardcastle, C. L. Hill, *Science* **2010**, *328*, 342–345.

[5] M. T. Pope in C *omprehensive Coordination Chemistry II*, *Vol. 4*, Elsevier, Oxford, **2004**, pp. 635–678.

[6] a) K. Wassermann, M. H. Dickman, M. T. Pope, *Angew. Chem.* **1997**, *109*, 1513–1516; *Angew. Chem. Int. Ed. Engl.* **1997**, *36*, 1445–1448; b) B. S. Bassil, M. H. Dickman, I. Römer, B. von der Kammer, U. Kortz, *Angew. Chem.* **2007**, *119*, 6305–6308; *Angew. Chem. Int. Ed.* **2007**, *46*, 6192–6195; c) A. Müller, P. Kögerler, C. Kuhlmann, *Chem. Commun.* **1999**, 1347–1358.

[7] a) P. Kögerler, B. Tsukerblat, A. Müller, *Dalton Trans.* **2010**, *39*, 21–36; b) A. M. Todea, A. Merca, H. Bögge, T. Glaser, L. Engelhardt, R. Prozorov, M. Luban, A. Müller, *Chem. Commun.* **2009**, 3351–3353.

[8] B. Botar, A. Ellern, R. Hermann, P. Kögerler, *Angew. Chem.* **2009**, *121*, 9244–9247; *Angew. Chem. Int. Ed.* **2009**, *48*, 9080–9083.

[9] B. Botar, A. Ellern, M. T. Sougrati, P. Kögerler, *Eur. J. Inorg. Chem.* **2009**, 5071–5074.

[10] A. Müller, S. K. Das, E. Krickemeyer, P. Kögerler, H. Bögge, M. Schmidtmann, *Solid State Sci.* **2000**, *2*, 847–854.

[11] S. Bertaina, S. Gambarelli, T. Mitra, B. Tsukerblat, A. Müller, B. Barbara, *Nature* **2008**, *453*, 203–207.

[12] J. W. Steed, J. L. Atwood, *Supramolecular Chemistry*, 2nd ed., Wiley, Hoboken, **2009**.

[13] S. Kitagawa, R. Kitaura, S.-I. Noro, *Angew. Chem.* **2004**, *116*, 2388–2430; *Angew. Chem. Int. Ed.* **2004**, *43*, 2334–2375.

[14] R. Contant, J. P. Ciabrini, *J. Chem. Res. Synop.* **1977**, 222.

[15] R. Contant, A. Tézé, *Inorg. Chem.* **1985**, *24*, 4610–4614.

[16] T. Lis, *Acta Crystallogr. Sect. B* **1980**, *36*, 2042–2046.

[17] A. J. Tasiopoulos, A. Vinslava, W. Wernsdorfer, K. A. Abboud, G. Christou, *Angew. Chem.* **2004**, *116*, 2169–2173; *Angew. Chem. Int. Ed.* **2004**, *43*, 2117–2121.

[18] Crystal data for **1a**: $H_{1374}K_{56}Li_{74}Mn_{40}O_{1568}P_{32}W_{224}$, at 173(2) K, $M=73547.20\,g\,mol^{-1}$, triclinic, space group $P\bar{1}$, $a=35.486(3)$ Å, $b=36.650(3)$ Å, $c=54.863(4)$ Å, $\alpha=80.738(1)°$, $\beta=83.694(2)°$, $\gamma=73.209(1)°$, $V=67268(8)$ Å^3, $Z=2$, μ(Mo-Kα) = 19.775 mm^{-1}, $2\theta_{max}=50.70°$, total 681413 reflections measured, 245793 unique ($R_{int}=0.1536$), 7582 parameters. ρ(max./min) = 5.13/−3.12 e Å^{-3}. The refinement converged to $R_1=0.0953$, $wR_2=0.2228$, and GOF = 1.013 with $I>2\sigma(I)$. Further details on the crystal structure investigations may be obtained from the Fachinformationszentrum Karlsruhe, 76344 Eggenstein-Leopoldshafen, Germany (fax: (+49) 7247-808-666; e-mail: crysdata@fiz-karlsruhe.de), on quoting the depository number CSD-422376.

[19] a) Z. Zhang, Y. Li, Y. Wang, Y. Qi, E. Wang, *Inorg. Chem.* **2008**, *47*, 7615–7622; b) S. Yao, Z. Zhang, Y. Li, E. Wang, *Dalton Trans.* **2009**, 1786–1791.

[20] S. G. Mitchell, S. Khanra, H. N. Miras, T. Boyd, D.-L. Long, L. Cronin, *Chem. Commun.* **2009**, 2712–2714.

[21] W. Liu, H. H. Thorp, *Inorg. Chem.* **1993**, *32*, 4102–4105.

[22] The W–O bond lengths in the Mn–O=W bridges of 1.69–1.76 Å only minimally exceed those of the terminal W=O groups.

[23] a) A. S. Assran, N. V. Izarova, U. Kortz, *CrystEngComm* **2010**, *12*, 2684–2686; b) Z.-M. Zhang, S. Yao, Y.-G. Li, Y.-H. Wang, Y.-F. Qi, E. Wang, *Chem. Commun.* **2008**, 1650–1652; c) S. Yao, Z. Zhang, Y. Li, E. Wang, *Dalton Trans.* **2010**, *39*, 3884–3889.

[24] S. S. Mal, U. Kortz, *Angew. Chem.* **2005**, *117*, 3843–3846; *Angew. Chem. Int. Ed.* **2005**, *44*, 3777–3780.

[25] A. Müller, M. T. Pope, A. M. Todea, H. Bögge, J. van Slageren, M. Dressel, P. Gouzerh, R. Thouvenot, B. Tsukerblat, A. Bell, *Angew. Chem.* **2007**, *119*, 4561–4564; *Angew. Chem. Int. Ed.* **2007**, *46*, 4477–4480.

[26] S. S. Mal, M. H. Dickman, U. Kortz, A. M. Todea, A. Merca, H. Bögge, T. Glaser, A. Müller, S. Nellutla, N. Kaur, J. Van Tol, N. S. Dalal, B. Keita, L. Najio, *Chem. Eur. J.* **2008**, *14*, 1186 – 1195.
[27] S. G. Mitchell, D. Gabb, C. Ritchie, N. Hazel, D.-L. Long, L Cronin, *CrystEngComm* **2009**, *11*, 36 – 39.
[28] S. G. Mitchell, C. Streb, H. N. Miras, T. Boyd, D.-L. Long, L. Cronin, *Nat. Chem.* **2010**, *2*, 308 – 312.
[29] M. Speldrich, H. Schilder, H. Lueken, P. Kögerler, *Israel J. Chem.* **2011**, *51*, 215 – 227.
[30] a) X. Fang, P. Kögerler, *Angew. Chem.* **2008**, *120*, 8243 – 8246; *Angew. Chem. Int. Ed.* **2008**, *47*, 8123 – 8126; b) H. N. Miras, G. J. T. Cooper, D.-L. Long, H. Bögge, A. Müller, C. Streb, L. Cronin, *Science* **2010**, *327*, 72 – 74.

